Astronomy & Astrophysics manuscript no. main
March 4, 2024

Atmospheric entry and fragmentation of small asteroid 2024 BX1: Bolide trajectory, orbit, dynamics, light curve, and spectrum

P. Spurný[1], J. Borovička[1], L. Shrbený[1], M. Hankey[2], and R. Neubert[3]

[1] Astronomical Institute of the Czech Academy of Sciences, Fričova 298, 25165 Ondřejov, Czech Republic
e-mail: pavel.spurny@asu.cas.cz
[2] American Meteor Society LTD, 54 Westview Crescent, Geneseo, New York 14454, USA
[3] Thüringer Landessternwarte Tautenburg, Sternwarte 5, D-07778 Tautenburg, Germany

Received 26 February 2024, Accepted xxx 2024

ABSTRACT

Asteroid 2024 BX1 was the eighth asteroid discovered shortly before colliding with the Earth.The associated bolide was recorded by dedicated instruments of the European Fireball Network and the AllSky7 network on January 21, 2024 at 0:32:38–44 UT. Here we report a comprehensive analysis of this instrumentally observed meteorite fall, which occurred as predicted west of Berlin, Germany. The atmospheric trajectory was quite steep with an average slope to the Earth's surface 75°.6. The entry speed was 15.20 km s^{-1}. The heliocentric orbit calculated from the bolide data agrees very well with the asteroid data. However, the bolide was fainter than expected for a reportedly meter-sized asteroid. The absolute magnitude reached −14.4 and the entry mass was estimated to 140 kg. The recorded bolide spectrum was low in iron from what an enstatite-rich meteorite was expected. Indeed, the recovered meteorites, called Ribbeck, were classified as aubrites. The high albedo of enstatite (E-type) asteroids can explain the size discrepancy. The asteroid was likely smaller than 0.5 meter and should be rather called a meteoroid. During the atmospheric entry, the meteoroid severely fragmented into much smaller pieces already at a height of 55 km under the aerodynamic pressure of 0.12 MPa. The primary fragments were then breaking-up again, most frequently at heights 39–29 km (0.9–2.2 MPa). Numerous small meteorites and up to four stones larger than 100g were expected to land. Within a few days of publishing the strewnfield dozens of meteorites were found in the area we predicted.

Key words. Meteorites, meteors, meteoroids – Minor planets, asteroids: individual: 2024 BX1

1. Introduction

On January 20, 2024 at 21:48 UT, Krisztián Sárneczky at the Hungarian Piszkéstető Observatory discovered a small asteroid 2024 BX1 (M. P. C. Staff 2024), which was on a collision course with Earth, as quickly confirmed by subsequent observations at more than ten other European observatories. As determined by imminent impact monitoring services such as JPL's Scout, ESA's Meerkat and MPC's internal warning system, the collision should have occurred around 0:33 UT in the area of Berlin, Germany (M. P. C. Staff 2024). This prediction was subsequently confirmed by the observation of a very bright bolide, which, from locations where it was clear and within range of the bolide, was seen by a large number of mostly casual observers, but was also recorded by instruments, both by casual witnesses and by systems specifically designed for the purpose of bolide observations.

Here we give a detailed analysis of this bolide using our standard methods as it was recorded by the various instruments of the European Fireball Network and partly by the cameras of the AllSky7 system. We will first describe what instrumental records we used and from where, then how we determined the atmospheric trajectory and heliocentric orbit of the body, its velocity and deceleration in the atmosphere, its luminosity and fragmentation, where its debris hit the Earth's surface, and also what its composition and physical properties were from the analysis of the spectra we took. Finally, we summarize the main results and compare them to both the pre-collisional analyses and to what meteorites were found. Since the meteorites have already been officially named Ribbeck (Meteoritical Bulletin 2024), we call the observed bolide the same hereafter.

2. Instruments and data

In this case, the bolide fortunately passed within range of the core of the European Fireball Network (EN), especially the Czech part of the EN, whose centre is located at the Ondřejov Observatory. Details regarding the current distribution of stations of this longest running fireball network in the world and the modern instruments it uses for bolide observations can be found in Spurný et al. (2017) or Borovička et al. (2022). This part of the EN currently consists of 21 stations located in the Czechia (15), Slovakia (4), and partly also Germany (1) and Austria (1). As to the observation of this event we were also lucky in the weather because it was clear over almost all stations. In order to accurately determine the bolide's trajectory in the atmosphere and its original orbit in the solar system (in this case it was only a confirmation of the already known orbit from pre-atmospheric observations), we used a total of 17 optical records (10 digital all-sky images and 7 video records) of which 15 were from the EN and 2 video records were from the German part of the AllSky7 network (Hankey et al. 2020). The image of the bolide taken by the video camera from the EN station Frýdlant is shown in Fig. 1. In addition, we used 3 radiometric and 3 spectral records exclusively from the EN network to determine asteroid properties. In Fig. 2, as an example of an important record,

Fig. 1. Composite image of the Ribbeck bolide from video footage taken by the IP camera at the Frýdlant station.

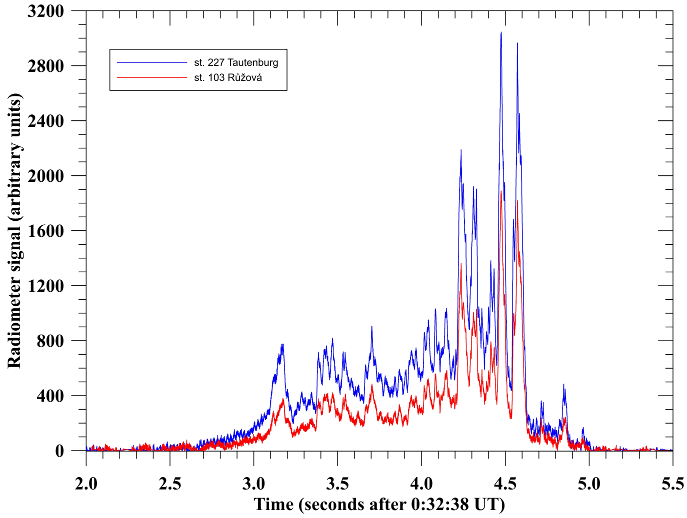

Fig. 2. Uncalibrated radiometric light curve of the Ribbeck bolide from stations 227 and 103. The reality of every visible detail in both LC's is confirmed by independent recordings from two stations 182 km apart.

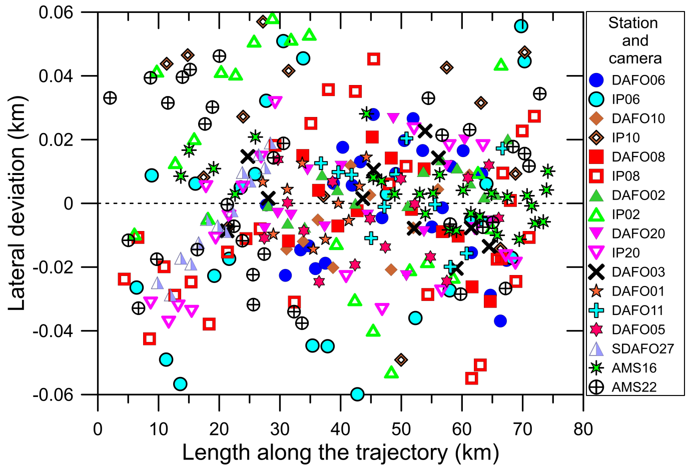

Fig. 3. Lateral deviations of all measured points on the luminous path of the fireball from all available records (17). Note that the Y-axis scale is highly enlarged and that one standard deviation for any point on the fireball trajectory is only 20 m.

we present the uncalibrated radiometric light curve (LC) of the bolide taken from the Tautenburg Observatory in Germany and the Czech station Růžová. This is used not only to determine the exact time of the bolide observation (determined with an accuracy corresponding to the temporal resolution of the radiometric record, which is 0.2 ms, i.e. 5000 samples per second), but mainly to determine the exact profile of the bolide luminosity (for example position and amplitude of individual flares) used to reveal the fragmentation in the atmosphere (see Section 4). This image also demonstrates the high fidelity of both records, which means, among other things, the realism of all the details in the displayed LCs. The signal at Tautenburg is higher because this station was closer to the bolide as shown in Table 1, where the data both for the position of all stations and for all optical records used are collected. The weights for the trajectory calculations were determined by giving double weight to the digital images compared to the video camera records because these images have higher resolution, only the very close Ketzür station was slightly favored due to the small distance from the bolide. The one-third weight for the spectral image (zero order) from Tautenburg was given because only a small part of the trajectory at the edge of the camera field of view was recorded. The velocity was determined only from the video cameras because, as the bolide was slow and relatively angularly short, the velocity in the images was not reliably measurable. The speed for mainly the first half of the trajectory was best measurable on the IP camera in Ondřejov and therefore has double the weight against the other IP cameras. For the AS7 cameras, the weight was further reduced because much of the bolide path was overexposed and very difficult to measure.In addition to these direct photographic, video, and radiometric records, detailed spectra were also obtained. The photographic spectrum was taken with the SDAFO wide-angle camera at Tautenburg and video spectra were taken with the IP cameras at Ondřejov and Kunžak. The spectral program of the EN was described in more detail in Borovička et al. (2019). All these records were used for the very comprehensive analysis of the bolide decribed in the following sections. Raw data from all records used are available upon request.

3. Trajectory and orbit

The bolide trajectory was computed by the least squares method of Borovička (1990). The trajectory was first assumed to be straight. Corrections for curvature due to gravity were applied at the end, when the linear trajectory and velocity were known. However due to very steep trajectory these corrections are very small. Good consistency of all positional measurements is demonstrated in Fig. 3, where the deviations of lines of sight from the trajectory are plotted. There is no significant systematic trend of any of the 17 records. The points are randomly mixed. All important trajectory data are provided in Table 2. The beginning and end points are the points where the bolide started and ceased to be visible on the records. The exact time corresponding to the beginning of the bolide shown in the Table 2 is $0^{h}32^{m}38^{s}.48$ UT. The ground projection of the atmospheric trajectory is shown in Fig. 4 and is relatively short (only 18.5 km) which is due to the large slope which was on average 75.6 degrees.

The geocentric radiant (α_G, δ_G) and heliocentric orbit were computed from the apparent radiant (α_R, δ_R) and entry velocity (v_∞) by the analytical method of Ceplecha (1987) with a small modification accounting for trajectory curvature described in Borovička et al. (2022). The entry velocity was determined from the dynamic fit along the first 30 km of fireball length (at heights above 64 km), where the fireball was well measurable

Table 1. Locations of the cameras, their distances to the fireball beginning and end, span of the recorded heights, total length, and used weights.

Station	Network No.	Camera	Coordinates (WGS84) Longit. E	Latitude N	h (m)	Distance (km) Beg	End	Height (km) Beg	End	Length (km)	W_T	W_V
Frýdlant	EN 6	DAFO	15.09047	50.91773	350	271.5	257.5	70.33	26.50	45.3	6	–
		IP				281.0	256.7	92.08	23.13	71.2	3	4
Polom	EN 10	DAFO	16.32225	50.35015	748	374.5	362.6	67.49	26.16	42.7	6	–
		IP				380.7	361.9	84.59	22.76	63.9	3	4
Jičín	EN 8	DAFO	15.34047	50.43439	279	322.7	310.6	70.53	27.47	44.5	6	–
		IP				330.1	309.7	90.36	23.16	69.4	3	4
Kunžak	EN 2	DAFO	15.20093	49.10729	656	442.2	433.7	71.50	27.17	45.8	6	–
		IP				447.0	433.2	89.77	23.93	68.0	3	4
Ondřejov	EN 20	DAFO	14.77994	49.91007	527	349.0	340.2	69.06	29.44	40.9	6	–
		IP				355.7	339.7	90.54	26.41	66.2	3	8
Růžová	EN 3	DAFO	14.28653	50.83411	348	246.7	233.4	74.12	30.36	45.2	6	–
Šindelová	EN 1	DAFO	12.59666	50.31740	595	265.0	261.5	68.95	49.28	20.3	6	–
Přimda	EN 11	DAFO	12.67807	49.66960	752	334.1	331.2	59.03	27.20	32.9	6	–
Kocelovice	EN 5	DAFO	13.83829	49.46724	525	370.1	363.9	67.74	27.12	42.0	6	–
Tautenburg	EN 27	SDAFO	11.71061	50.98168	338	205.5	200.3	85.61	65.38	20.9	2	–
Ketzür	AMS 16	AS7	12.63124	52.49502	45	82.5	26.4	80.52[a]	21.26	61.2	4	1
Lindenberg	AMS 22	AS7	14.12152	52.20867	125	157.4	113.9	93.32	22.60	73.0	3	1

[a] entering field of view

Notes. The abbreviations used - EN means European Fireball Network, AMS means American Meteor Society, AS7 means AllSky7 Global Network, DAFO means Digital Autonomous Fireball Observatory which produces all-sky photographic images and radiometric light curves, SDAFO is spectral version of the DAFO, IP means Internet Protocol video camera, (W_T) and (W_V) are trajectory and velocity weights.

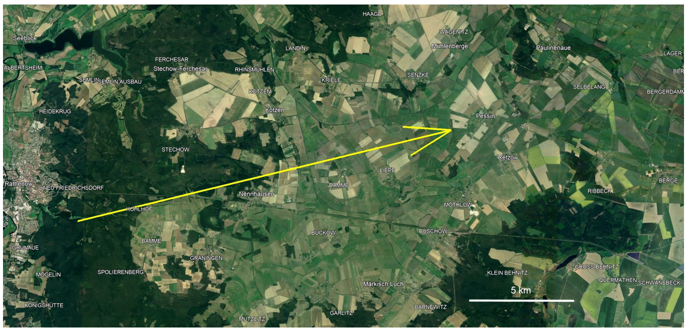

Fig. 4. Ground projection of the atmospheric trajectory of the Ribbeck bolide. Note that the average slope was 75°.6. The background map is from Google Earth. North is up.

Table 2. Atmospheric trajectory data of the Ribbeck bolide.

	Beginning	Terminal
Height (km)	93.315 ± 0.004	21.256 ± 0.003
Longitude (° E)	12.38009 ± 0.00008	12.64232 ± 0.00006
Latitude (° N)	52.58959 ± 0.00006	52.63502 ± 0.00005
Slope (°)	75.557 ± 0.008	75.74 ± 0.02
Azimuth (°)	74.01 ± 0.03	74.22 ± 0.03
L (km) / T (s)	74.42/ 5.95	

Notes. Height is above the sea level. Azimuth is taken from south. L is the length and T is the duration of the recorded trajectory.

and severe fragmentation has not yet begun. The initial mass was set to the value obtained from light curve modeling (Sect. 4).

The results are given in Table 3. In addition, the orbital elements determined from pre-collision observations are presented in the right column, providing a unique opportunity to compare the results of the two independent methods. It is obvious and also generally accepted that the orbit determined from observations in interplanetary space is significantly more accurate. However, in this case the bolide data are also very accurate and, most importantly, the agreement of all elements is within a fraction of one standard deviation determined for the bolide data. The only parameter that differs more than the others is the longitude of the ascending node, which in the method we use (Ceplecha 1987) corresponds to the length of the Sun at the moment of the body's collision with the Earth. The problem of this simplification has already been identified by Clark and Wiegert (2011) and is also present here. But since the longitude of the ascending node is not a crucial parameter in terms of the description of the orbit in the solar system and does not reduce the accuracy of the orbit determination itself, this small inaccuracy is not that important. On the contrary, the perfect agreement of all other elements is a very important result that fully legitimizes the use of the Ceplecha's analytical method.

4. Light curve and fragmentation

The calibrated bolide light curve as a function of height is presented in Fig. 5. The light curve at the beginning and end was measured using three IP video cameras. These cameras became strongly saturated during the bolide bright phase. The medium brightness part was measured on the photographic DAFO camera in Frýdlant. The absolute calibration (using stars) from all these systems is in good agreement. The bright part of the bolide was well covered by the radiometers, which are linear detectors with high dynamic range. The absolute magnitude scale was adjusted to match the camera data.

The bolide reached the maximum brightness of −14.4 absolute magnitude in two almost equally bright flares at heights 35.2 and 33.9 km. Many other flares of various amplitudes occurred between the heights 54 – 29 km. Another, and the last observed flare occurred at 24.5 km.

The flares are signs of meteoroid fragmentations, at which fine dust was released and quickly vaporized. Numerous macro-

Table 3. Apparent and geocentric radiant and velocity and orbital elements (J2000.0) of the Ribbeck meteorite fall.

	Bolide	Asteroid
v_∞ (km/s)	15.199 ± 0.008	-
α_R (deg)	119.546 ± 0.011	-
δ_R (deg)	46.739 ± 0.007	-
α_G (deg)	114.592 ± 0.013	-
δ_G (deg)	44.902 ± 0.009	-
v_G (km/s)	10.476 ± 0.012	-
a (A.U.)	1.3344 ± 0.0007	1.3343797
e	0.3740 ± 0.0004	0.3740191
q (A.U.)	0.83534 ± 0.00016	0.8352962
Q (A.U.)	1.8334 ± 0.0015	1.8334632
ω (deg)	243.602 ± 0.016	243.60428
Ω (deg)	300.092	300.14142
i (deg)	7.264 ± 0.009	7.26653
P (years)	1.5414 ± 0.0012	1.5414134

Notes. Orbital elements from ground-based telescopic observations of the asteroid in space for the epoch 2023 Sept. 13.0 TT are in the right column for direct comparison (MPEC 2024-B76)

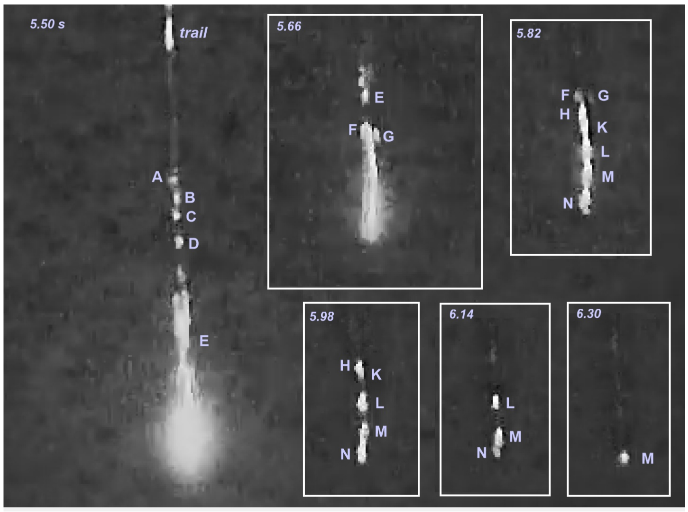

Fig. 6. Bolide images on six individual frames from the ALLSKY7 AMS 16 video. Fragments which could be measured are marked with capital letters. Time is given in seconds from 0:32:38 UT.

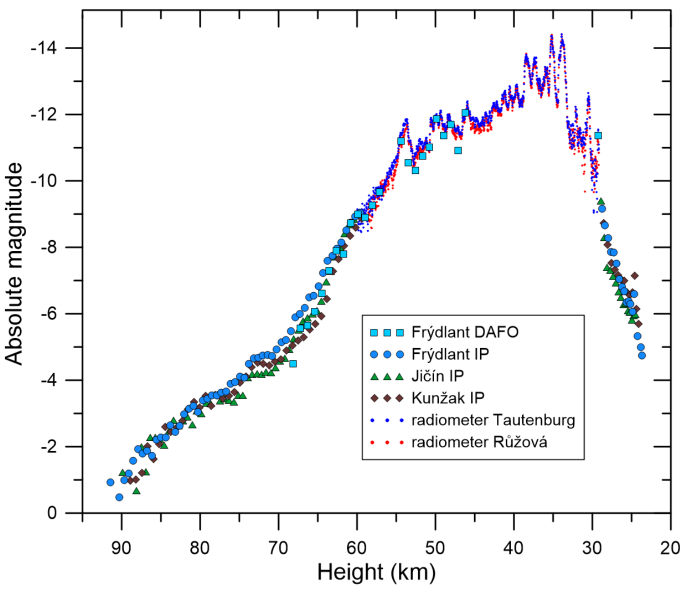

Fig. 5. Calibrated light curve as a function of height combined from various instruments.

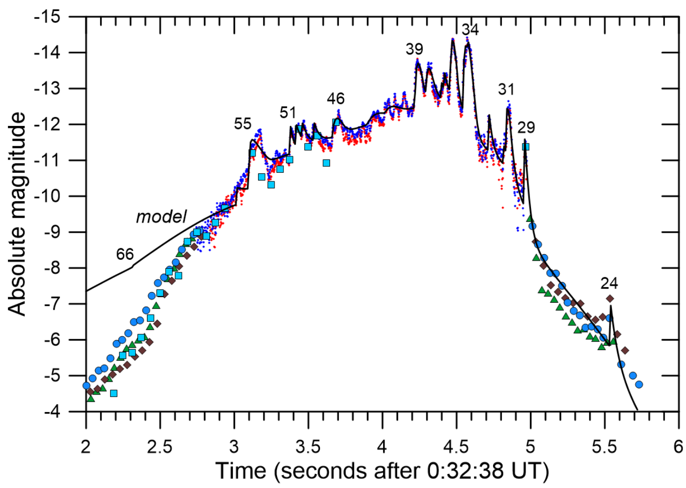

Fig. 7. Observed (symbols) and modeled (solid line) light curve as a function of time. The symbols are the same as in Fig. 5. The numbers give approximate heights in km of selected features on the light curve.

scopic fragments are directly visible on video records taken from close distance (Fig. 6).

We have modeled the fragmentation using the Semiempirical Fragmentation Model described in Borovička et al. (2020). The inputs were the light curve and the dynamics (deceleration) of the bolide as a whole and of individual fragments. Since the spectrum was poor in iron (see Sect. 6) and iron contributes many spectral lines, the assumed luminous efficiency (at 15 km s^{-1}) was decreased to 4% for high mass limit and 2% for fine dust from the normally used 5% and 2.5%, respectively. The product of the drag and shape coefficient was set to $\Gamma A = 0.7$, the meteoroid density was assumed to be $\delta = 3100$ kg m^{-3}, and the ablation coefficient was fixed at $\sigma = 0.005$ kg MJ^{-1}. The atmospheric density model CIRA72 was used.

The modeled light curve is presented in Fig. 7. To fit all produced radiation, the initial meteoroid mass was set to 140 kg. The beginning of the bolide, when the meteoroid was heating up and the ablation was not yet in its full stage, cannot be described by the model. It seems that some fragmentation, more precisely gradual dust loss, started already during this phase, at a height of 66 km. It is evidenced by a change in slope of the light curve but also a long wake of the bolide seen in the videos at heights 64 – 57.5 km. The first major, and in fact catastrophic, fragmentation started at a height of 55 km and was demonstrated by the first flare. In addition, significant deceleration of the bolide started after the time of this fragmentation as shown in Fig. 8. The deceleration corresponds to the mass of largest fragments of about 5 kg. At the times 4 – 4.5 s, the measured lag behind the constant velocity course was even larger than modeled on most videos (Fig. 8). It suggests that the majority of fragments were even smaller (1–2 kg) and the photocenter was shifted behind the leading fragments.

The fragments produced at 55 km fragmented further at lower heights. As evidenced by the flares, some minor fragmentations occurred at heights 51–40 km and major fragmentation ocurred at heights 39–29 km. Dust was released either immediately or quickly because the flares have high amplitude and short duration. To estimate the masses and heights of origin of the surviving fragmentation products, the dynamics of the frag-

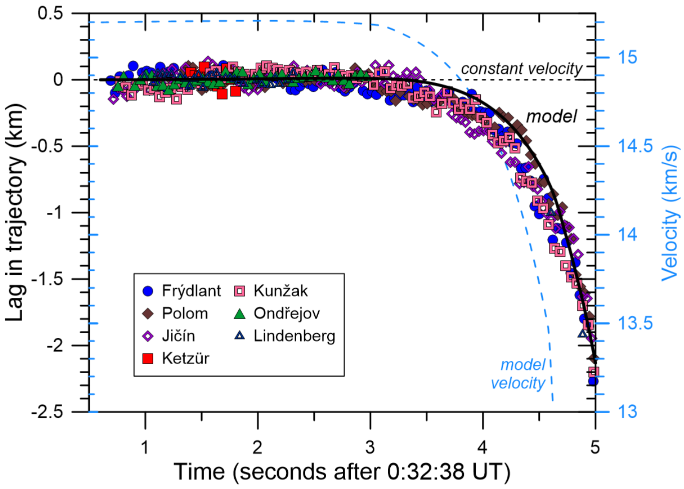

Fig. 8. Lag in trajectory with respect to constant velocity of 15.199 km s^{-1} as a function of time. Symbols represent measurements on individual videos. Solid line is the lag model for the leading fragment. The dashed line (with scale on the right) is the corresponding model velocity.

Table 4. List of the most important fragmentations.

Time (s)	Height (km)	Aerodynamic pressure (MPa)	Parent mass (kg)	Product mass (kg)
2.32	66	0.03	140	138
3.02	55.8	0.11	138	115
3.10	54.6	0.12	115	5.5
4.22	38.5	0.87	5.1	2.2
4.30	37.7	1.07	4.4	1.5
4.42	35.8	1.32	3.9	0
4.45	35.4	1.40	4.6	1.4
4.58	33.7	1.74	4.9	0.13
4.72	32.0	1.93	1.3	0.5
4.84	30.6	2.17	1.89	0.99
4.96	29.3	2.04	0.44	0.04
5.54	24.4	1.79	0.78	0.07

Notes. The mass of the body before fragmentation and the mass of the largest fragmentation product in our model are given in the last two columns.

ments seen at the Ketzür video was measured and fitted. We have also measured the fragments on the video taken by Michael Aye (@allplanets) in Berlin using a handheld mobile phone and published on the Internet[1]. An attempt to reconstruct the individual fragment trajectories in space was not successful since the measured trajectories are short and data precision is not high enough for such a task. All fragments were therefore supposed to follow the same trajectory.

Table 4 gives the list of the most important fragmentation events. The time (counted from 0:32:38 UT), height, aerodynamic pressure computed as $p = \rho v^2$, where ρ is atmospheric density and v is velocity, the mass of the fragmenting body and the mass of the largest fragmentation product are given. Of course, the fragmentation sequence could not be determined unambiguously. Moreover, fragmentations of different fragments likely occurred nearly simultaneously. Listed in the table are the fragmentations of the largest fragments in our model. The masses of the fragmentation products were partly derived from

[1] https://mastodon.online/@michaelaye/111791284304249289

Table 5. Individually observed fragments (see Fig. 6).

Designation	Origin height (km)	Initial mass (g)	Meteorite mass (g)
A	43.0	16	9
B	41.4	19	11
C	38.5	14	8
D	38.5	26	15
E	32.0	40	25
F	33.7	130	85
G	29.3	40	30
H	35.3	270	170
K	32.0	180	120
L	32.0	300	210
M	35.4	660	410
N1[a]	30.6	990	–
N	24.4	70	60

[(a)] N1 is the precursor of N.

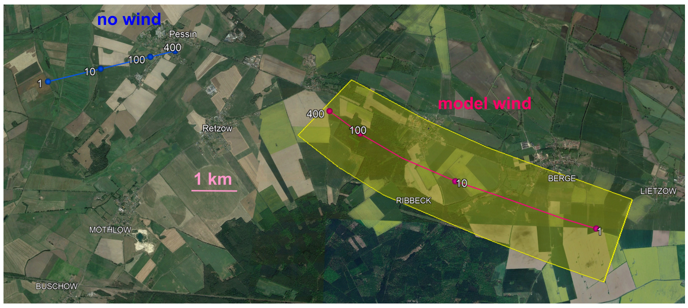

Fig. 9. Map of computed meteorite fall locations for the hypothetical case of no atmospheric wind (blue) and with the usage of the ALADIN wind model (red). The numbers show meteorite masses in grams and are valid for spherical meteorite shapes. An estimated uncertainty area is shown in yellow for the wind case. The 400 g point lies at 52.°6285 N, 12.°7200 E. The background map is from Google Earth. North is up.

the dynamics of directly visible fragments (Fig. 6). Their parameters are given in Table 5. The earliest visible fragments were produced at heights around 40 km and had masses in the range ≈ 15 – 25 g. They possibly produced meteorites in the 10 g mass range. The largest piece which emerged from multiple fragmentations at heights 35 – 29 km (marked N1) had initially almost 1 kg mass. However, it lost most its mass in another break-up at 24.4 km and only about 60 g meteorite was left. The late break-up occurred when the aerodynamic pressure was already decreasing (the velocity at the break-up was only 6.6 km s^{-1}). The largest fragment which survived at least until the end of the bolide luminous phase (M) had a mass of about 400 g.

5. Meteorite strewn field

The expected meteorite landing positions were computed using the dark flight procedure of Ceplecha (1987). The procedure was started when fragment velocity dropped to 2 km s^{-1}. At that time the ablation surely ceased. The largest fragment M was visible on the video (and thus ablating) down the velocity of 2.7 km s^{-1}. The atmospheric pressure, temperature, and wind profile for 0 UT and 1 UT was kindly provided to us by R. Brožková from the Czech Hydrometeorological Institute using the ALADIN (Aire Limitée Adaptation dynamique Développement InterNational) weather forecast model.

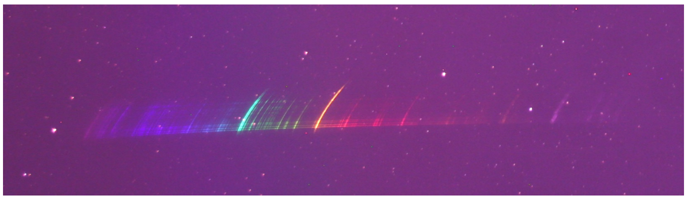

Fig. 10. Original color image of the Ribbeck bolide spectrum with stars in the background. The bolide moved from top to bottom. The wavelengths increase from left to right. The curvature of spectral lines is due to the geometry of the fish-eye lens.

A map of the computed strewn field is shown in Fig. 9. For comparison, the computation without wind is shown as well. In that case, the meteorites would be distributed along a line in the direction of bolide flight with large meteorites further ahead. The wind, blowing from western to northwestern directions, completely changed the situation. The meteorites were distributed along the wind direction with the smallest meteorites blown further away. Note that the distance flown depends not only on meteorite mass but also on shape, which affects the drag coefficient during the dark flight (Towner et al. 2022). The masses given in Fig. 9 are for spherical shapes. Brick-like or irregularly shaped meteorites may have been transported further east.

Fig. 9 shows also the uncertainty in the meteorite line, which is mostly due to the uncertainty in the wind. The wind can exhibit variations in time, which the wind model cannot account for. Some spread of meteorites can be also expected due to ejection angles during the fragmentations and due to aerodynamic effects. Some of the meteorites can therefore lie outside the marked area.

The number of meteorites is uncertain. There were probably four meteorites larger than 100 g at the end of ablation (Table 5). Nevertheless, further break-ups during the dark flight cannot be excluded. Smaller meteorites were surely more numerous than given in Table 5 because there are unresolved fragments in the video, for example between fragments E and D (Fig. 6). There may be several dozens meteorites of masses 10 – 100 g and up to several hundreds of those between 1 – 10 g.

Our strewn field map was in fact made available already on January 22 and dozens of meteorites were already found in the designated area (Meteoritical Bulletin 2024). The exact locations of most of them are, however, not known to us at the time of writing.

6. Spectrum and composition

The bolide spectrum taken by the SDAFO at Tautenburg is shown in Fig. 10. The bolide was low over horizon and angularly short but bright enough to produce nice spectral image. The bright green line belongs to magnesium and the yellow line is of sodium.

The inspection of the spectrum is best done in comparison with another spectrum. In Fig. 11, the spectrum of the bright part of the bolide (heights 34–39 km) is plotted together with the spectrum of Kindberg bolide at similar heights (38–40 km). The Kindberg bolide lead to the fall of ordinary chondrite of type L6 in Austria on November 19, 2020 (Gattacceca et al. 2022). The spectrum was taken by another SDAFO of the EN network in Churáňov station. Both bolides had similar speeds.

Although the same Mg and Na lines are the brightest lines in both spectra, there is a significant difference in that the Kindberg spectrum is otherwise dominated by numerous Fe lines, the brightest of them lying between 5250–5500 Å. In Ribbeck, the Fe lines are much fainter or absent and many lines of Mg, Na, and Ca are seen. Lines of K, Li, Mn, Cr, and Ti are also visible. All these lines are present in Kindberg as well but are less conspicuous. Bands of AlO and MgO oxides, previously seen only in the very bright Benešov bolide (Borovička & Berezhnoy 2016), are also visible, while FeO is present in Kindberg and not in Ribbeck. Lines of Al seem to be bright in Ribbeck but are blended with Ca^+ and difficult to measure.

A rough estimate of abundances of neutral atoms in the radiating plasma indicates that Fe was depleted 30–50× relative to Mg in Ribbeck in comparison with Kindberg. Li, Ca, and Ti have nearly the same ratio to Mg. K may be 2× underabundant, Mn 2–3× and Cr 8× underabundant. Na seems to be 2–3× enhanced in Ribbeck. A more rigorous abundance determination will be done in the future. Nevertheless, strong depletion of Fe is evident and pointed out an enstatite ($MgSiO_3$) rich material even before the meteorites were found.

7. Discussion and conclusions

The combination of pre-collision observation of an asteroid, the associated bolide, and the recovery of meteorites, is the fourth such case in history. However, 2024 BX1 is clearly the best documented case of this kind. The first such case was the observation of the asteroid 2008 TC3 associated with the Almahata Sitta meteorite fall in Sudan on 7 October 2008 (Jenniskens et al. 2009). The second similar case was associated with the asteroid 2018 LA fall in Botswana on 2 June 2018 (Jenniskens et al. 2021). However, for both of these falls there were only limited data for the bolide. The third such case was the fall of asteroid 2023 CX1 in France on 13 February 2023 (Vida et al. 2023). For this case there is already significantly better documentation of the bolide but the data from France are mostly amateur records even though it was within the FRIPON network(Colas et al. 2020), which however did not properly observe the bolide. Fortunately, the 2024 BX1 bolide occurred within the range of the EN network, which provided precise and multi-instrumental data including detailed radiometric light curve and spectrum. The video data from the AllSky7 network, taken from a closer distance, were also useful, especially for measuring the fragments, and proved to be reliable when properly reduced.

There are two main areas where asteroid and bolide data that can be directly compared, namely the trajectory in the atmosphere and especially the original orbit in the solar system. Obviously, the atmospheric trajectory of the body will be more accurately determined from observations of its passage through the atmosphere, i.e. from direct data from the bolide networks. This is summarized in Section 3 in Table 2 and Fig. 3, and it can be seen that the position of the trajectory in the atmosphere is determined to an accuracy of about 20 meters, which can hardly be given by pre-collisional observations. On the other hand, it is generally accepted that the determination of the orbit in the solar system is mainly the domain of observations from telescopes when the body is in interplanetary space. This is practically for the first time, where we can compare the two methods independently. This comparison presented in Table 3 shows that both methods give very similar results, i.e., that all elements determined from bolide observations fit within one standard deviation (for most of elements it is only small fraction of it) to the elements, determined before collision. Of course, these are more precise. Therefore, it is evident that the bolide data, if properly and thoroughly processed, can give a perfectly plausible description of the orbit in the solar system. This is one of the absolutely crucial results, which, moreover, substantially supports the plau-

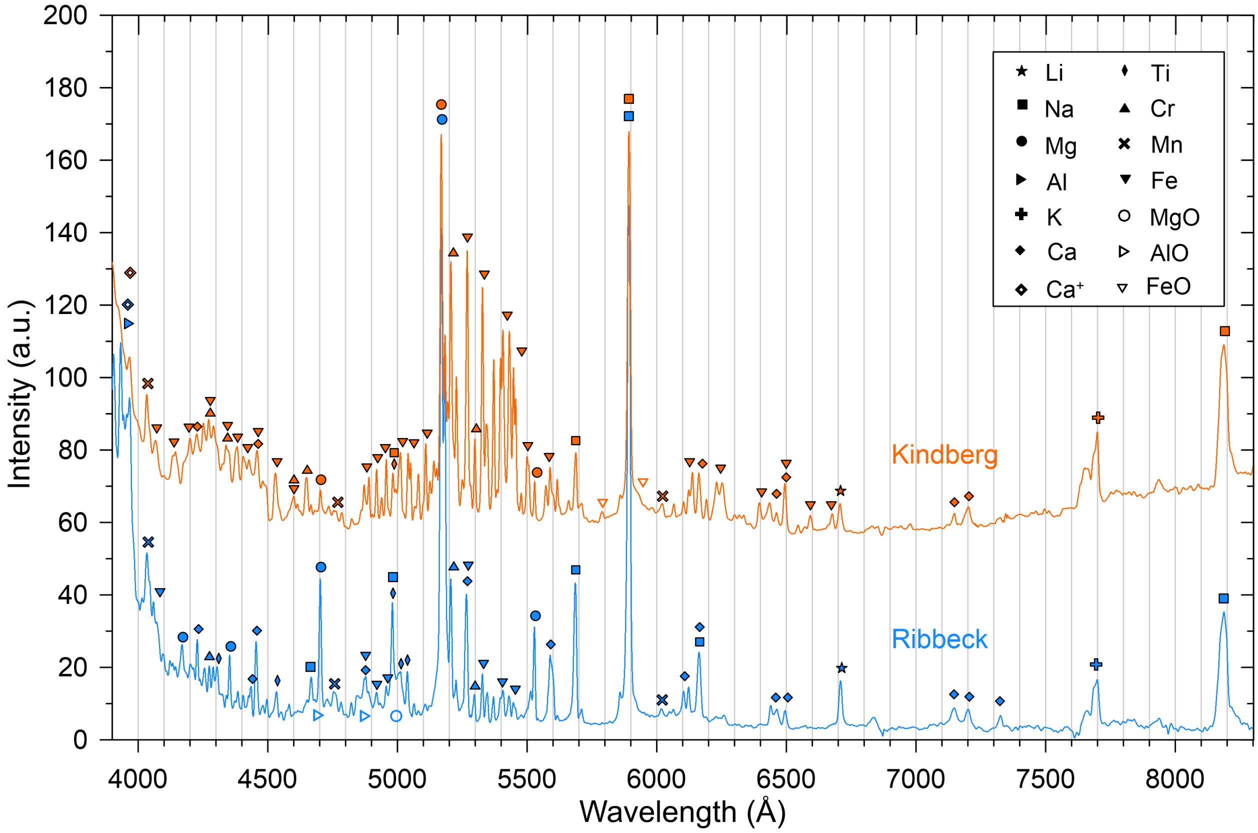

Fig. 11. Comparison of spectra of the Kindberg and Ribbeck (2024 BX1) bolides in the range 3900 – 8300 Å. The Kindberg spectrum has been vertically offset by 50 units. Atoms, ions, and molecules contributing to the observed lines and bands are identified using the symbols from the legend. In some cases, two atoms contribute to a line. In other cases, one symbol is used for two or more neighboring lines of the same atom(s).

sibility of most of the other conclusions from the bolide analysis as well.

We can also compare the size determination. Asteroid 2024 BX1 observed in space had an absolute magnitude 32.84 (M. P. C. Staff 2024). From that, the size was estimated and widely reported before the impact as about one meter. The corresponding asteroid mass would be about 1700 kg. The estimate was based of the usual albedo of the most common S-type asteroids of 0.15. The observed bolide, though surely very nice, was, nevertheless, much fainter than it could be expected for such a mass. Indeed, our initial mass estimate based on the bolide radiation was of the order of 100 kg only. After inspecting the spectrum, we found that the material was significantly poorer in iron than usual meteoroids. A composition rich in enstatite was suggested. The high albedo of about 0.50 of enstatite rich E-type asteroids and aubrite meteorites (Clark et al. 2004; Dibb et al. 2022) would change the asteroid size estimate to 0.50 m. Subsequently, the meteorites were recovered and indeed classified as aubrites (Meteoritical Bulletin 2024). It was the first time when the meteorite type was predicted from the bolide spectrum. Our final estimate of the asteroid size from the bolide model is 0.44 m, for the mass 140 kg and typical aubrite density 3100 kg m^{-3} (Britt & Consolmagno 2003). Considering the uncertainties in the actual luminous efficiency, albedo, and bulk density, we consider the agreement between bolide and asteroid data good.

A simple method to estimate meteoroid diameter from the bolide absolute magnitude and velocity at the height of 60 km was recently proposed by Johnston & Stern (2024). From their formula and the Ribbeck magnitude of −9 at 60 km, we obtained a diameter of 34 cm. That is too low in our opinion and the reason may again be the lack of iron. Apart from sodium, iron lines are among the brightest in the spectra of bolide early parts, while Mg, and especially Ca, appear later on. Ribbeck was therefore fainter at 60 km than an ordinary bolide. Magnitude −9.7 would be expected for a diameter of 44 cm according to the formula of Johnston & Stern (2024).

Given the size much lower than one meter, 2024 BX1 should be referred rather as a meteoroid than an asteroid according to the adopted definitions of the International Astronomical Union commission F1 (Koschny & Borovička 2017). Regardless the term, 2024 BX1 was probably the smallest natural body ever observed telescopically in space.

The atmospheric entry was characterized by extensive fragmentation. Ordinary chondrites usually fragment in two distinct phases, at 0.04–0.12 MPa and 0.9–5 MPa (Borovička et al. 2020). The behavior of 2024 BX1 was similar with two differences. First, numerous fragmentations, though minor, occurred also between the two phases. Second, the first phase was extraordinary severe. The masses of the largest surviving fragments were less than 5% of the original mass. Among the bodies studied by Borovička et al. (2020), only Benešov meteoroid fragmented so severely at the beginning. In that case it was not so surprising because Benešov was a conglomerate of different meteorite types (Spurný et al. 2014). It seems that 2024 BX1 was a weekly cemented conglomerate of small boulders, i.e. type C material as defined by Borovička et al. (2020). The boulders themselves were heavily cracked (type B material) and most of them disintegrated into dust at later stages of atmospheric entry. Only small percentage of the original mass reached the ground as meteorites, mostly small ones. Maximally four meteorites larger than 100 g could be expected.

Ribbeck was not a particularly large meteorite fall and yet the meteoroid was discovered in space. This indicates that as the efficiency of asteroid discoveries increases and the bolide network expands, more such events can be expected. We have shown that valuable and accurate results can be obtained from bolide observations, provided the correct procedures are used. However, in terms of bolide observations, this means that the data acquired must be of sufficient quality and complexity. This requires multi-instrument observations that include radiometers and spectroscopy in addition to standard camera systems. Only such observations can provide the most complete description of not only the atmospheric trajectories and heliocentric orbits but also the physical properties and composition of meteoroids.

Acknowledgements. We thank Radmila Brožková from the Czech Hydrometeorological Institute for providing us the atmospheric wind model data and operators Sirko Molau (AMS16 Ketzür) and Andre Knöfel (AMS22 Lindenberg) for providing video recordings of the AllSky7 network from their sites. We are grateful to Peter Brown for his quick and helpful review. This work was supported by grant no. 24-10143S from the Czech Science Foundation. The institutional research plan is RVO:67985815.

References

Borovička J. 1990, Bull. astr. Inst. Czechosl., 41, 391
Borovička, J., & Berezhnoy, A. A. 2016, Icarus, 278, 248
Borovička, J., Spurný, P., & Shrbený, L. 2019, in Proc. Int. Meteor Conf., Pezinok-Modra, Slovakia, 30 August – 2 September 2018 (R. Rudawska et al., eds.), p. 28
Borovička, J., Spurný, P., & Shrbený, L. 2020, AJ, 160:42
Borovička, J., Spurný, P., Shrbený, L., et al. 2022, A&A, 667:A157
Britt, T. D. & Consolmagno, G. J. 2003, Meteorit. Planet. Sci., 38, 1161
Ceplecha, Z. 1987, Bull. astr. Inst. Czechosl., 38, 222
Clark, B. E., Bus, S. J., Rivkin, A. S. et al. 2004, J. Geophys. Res., 109, E02001
Clark, D. L., & Wiegert, P. A. 2011, Meteorit. Planet. Sci., 46, 1217
Colas, F., Zanda, B., Bouley, S., et al. 2020, A&A, 644, A53
Dibb, S. D., Bell III, J. F. & Garvie, L. A. J. 2022, Meteorit. Planet. Sci., 57, 1570
Gattacceca, J., McCubbin, F. M., Grossman, J. et al. 2022, Meteoritical Bulletin No. 110, Meteorit. Planet. Sci., 57, 2102
Hankey, M., Perlerin, V. & Meisel, D. 2020, Planet. Space Sci, 190, 105005
Jenniskens, P., Shaddad, M. H., Numan, D. et al. 2009, Nature, 458, 7237, 485
Jenniskens, P., Gabadirwe, M., et al. 2021, Meteorit. Planet. Sci., 56, 844
Johnston, C. O., & Stern, E. C. 2024, Icarus, 408, 115807
Koschny, D., & Borovicka, J. 2017, WGN, J. IMO, 45, 91
M. P. C. Staff 2024, Minor Planet Electronic Circular, 2024-B76
Meteoritical Bulletin Database entry 2024, to be published in Meteorit. Planet. Sci., https://www.lpi.usra.edu/meteor/metbull.php?code=81447
Spurný, P., Haloda, J., Borovička, J., et al. 2014, A&A, 570:A39
Spurný, P., Borovička, J., Mucke, H., Svoreň, J. 2017, A&A, 605:A68
Towner, M. C., Jansen-Sturgeon, T., Cupák, M., et al. 2022, Planet. Sci. J., 3:44
Vida, D., Egal, A., Brown, P. G., et al. 2023, Asteroids, Comets, Meteors Conference 2023 (LPI Contrib. No. 2851), abstract # 2049